Published in final edited form as:

ACS Appl Mater Interfaces. 2018 October 10; 10(40): 33847–33856. doi:10.1021/acsami.8b09751.

Temperature-Responsive Magnetic Nanoparticles for Enabling Affinity Separation of Extracellular Vesicles

Ramon Jauregui[†], **Selvi Srinivasan**[†], **Lucia N. Vojtech**[‡], **Hilary S. Gammill**[‡], **Daniel T. Chiu**[‡,§], **Florian Hladik**[‡], **Patrick S. Stayton**[†], and **James J. Lai**[*,†]

[†] Department of Bioengineering, Seattle, Washington 98195, United States

[‡] Department of Obstetrics and Gynecology, Seattle, Washington 98195, United States

[§] Department of Chemistry, University of Washington, Seattle, Washington 98195, United States

Abstract

Small magnetic nanoparticles that have surfaces decorated with stimuli-responsive polymers can be reversibly aggregated via a stimulus, such as temperature, to enable efficient and rapid biomarker separation. To fully realize the potential of these particles, the synthesis needs to be highly reproducible and scalable to large quantity. We have developed a new synthesis for temperature-responsive magnetic nanoparticles via an in situ coprecipitation process of Fe^{2+}/Fe^{3+} salts at room temperature with poly(acrylic acid)-*block*-poly(*N*-isopropylacrylamide) diblock copolymer template, synthesized via the reversible addition− fragmentation chain-transfer polymerization method. These particles were 56% polymer by weight with a 6.5:1 Fe/COOH ratio and demonstrated remarkable stability over a 2 month period. The hydrodynamic diameter remained constant at ~28 nm with a consistent transition temperature of 34 °C, and the magnetic particle separation efficiency at 40 °C was ≥95% over the 2 month span. These properties were maintained for all large-scale synthesis batches. To demonstrate the practical utility of the stimuli-responsive magnetic nanoparticles, the particles were incorporated into a temperature-responsive binary reagent system and efficiently separated a model protein biomarker (mouse IgG) as well as purified extracellular vesicles derived from a human biofluid, seminal plasma. The ease of using these particles will prove beneficial for various biomedical applications.

Graphical Abstract

[*]**Corresponding Author** jilai@u.washington.edu. Tel: (206) 221-5168. Fax: (206) 616-3928.

Author Contributions

The manuscript was written through contributions of all authors. All authors have given approval to the final version of the manuscript.

▮ ASSOCIATED CONTENT

Supporting Information

The Supporting Information is available free of charge on the ACS Publications website at DOI: 10.1021/acsami.8b09751.

Table to illustrate mNP synthesis with various Fe/ COOH ratios; polymer ^{1}H NMR spectra; polymer GPC chromatograms; solution images for the mNP synthesis; TEM images of the synthesized mNPs; could point measurement for the mNP transition temperature; DLS data showing the mNP particle size distribution over a 2 month storage; fluorescence measurements of the extracellular vesicle supernatants after the separation via the binary reagent system (PDF

The authors declare the following competing financial interest(s): J. J. Lai and P.S. Stayton are co-founders and consultants for Nexgenia Inc., a company that has licensed similar separation technology, however this work was conducted independently of Nexgenia Inc. under NIH support.

None of the other authors have potential conflicts of interest.

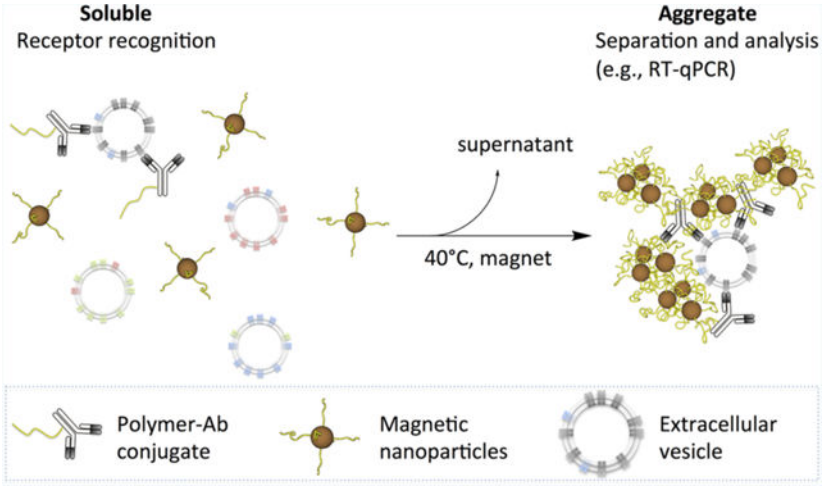

Keywords

magnetic nanoparticle; extracellular vesicle; stimuli-responsive polymer; diblock co-polymer; biomarkers

INTRODUCTION

The capture and separation of biomolecules can be a valuable tool in identifying disease; however, such desirable biomarkers are usually present in very low concentrations in biofluids.[1,2] The immunoaffinity capture mechanism has proven effective at concentrating low-abundance biomarkers, making use of the interaction between antibodies and the target molecule.[3] The magnetic microbeads with immobilized antibodies have been utilized for immunoprecipitation to enable clinical applications, like immunoassays and other life science research.[4,5] Particles in the micrometer range enable rapid magnetic separation but compromise biomarker recognition kinetics and efficiency.[2] Much smaller magnetic nanoparticles (mNPs) of 25 nm diameter or less are well suited for biomarker recognition,[6] however, limited magnetophoretic mobility due to small particle size leads to slow magnetic separation lasting several hours.[7,8] Our group and others have developed stimuli-responsive mNPs to overcome this challenge and meet the need to balance recognition efficiency with high-throughput scalability.[2,9–16] We decorate the mNP surfaces with stimuli-responsive polymers, which drive the particles to reversibly aggregate via temperature or pH shift. Although the unaggregated mNPs respond to the magnetic field sluggishly, the aggregates can be rapidly captured in a few minutes via a modest magnetic field. Additionally, the capability of “reversible aggregation” has been demonstrated in our previous publication via a microfluidic device using pH as the stimulus.[10] Prior to the separation, the particles with bound protein analytes were aggregated by adjusting the solution to pH 7.4. In the microchannel, the aggregates in low pH solution response to the magnetic field by crossing the interface into a higher pH stream. Then, the aggregates redissolved in the higher pH environment and the soluble particles could not be captured by the magnetic field. Therefore, the purified protein markers could be continuously collected at the outlet. In this particular case, the reversible aggregation was demonstrated using pH as the stimulus.

Compared to the magnetic microbead (≥1000 nm) with immobilized antibodies, the stimuli-responsive mNPs can achieve rapid and highly efficient biomarker recognition while maintaining the rapid magnetic separation. Our previous work has demonstrated that the stimuli-responsive mNPs reagent system could achieve highly efficient biomarker recognition almost instantaneously, where as the magnetic microbeads, such as Dynabeads, took up to an hour of incubation to achieve the same level of biomarker recognition.[2] The significant difference in the binding kinetics likely reflected some combinations of differences in diffusion properties, hydrodynamic factors, and sizes.

To fully realize the potential of stimuli-responsive mNPs, highly reproducible synthetic approaches that enable precise control of particle properties for scale-up production are needed. Various methods have been utilized for the synthesis of mNPs.[17–25] The functionalization required to provide the stimuli-responsiveness can be carried out either simultaneously to or after synthesis of the mNPs.[26–32] In either case, controlling particle size and surface coverage with polymer remains challenging. Our group previously published the synthesis of stimuli-responsive mNPs via the one-step thermal decomposition method.[2,9–12] In this process, poly(*N*-isopropylacrylamide) (pNIPAAm) homopolymers with a hydrophobic end group (dodecyl) formed polymeric micelles that were then loaded with $Fe(CO)_5$ and heated at 190 °C for 5 h. This yielded temperature-responsive γ-Fe_2O_3 nanoparticles, but prolonged high-temperature heating compromises reproducibility and scale-up manufacturing.

To overcome this problem, here we report a new method where the particles are simultaneously synthesized and functionalized in the presence of temperature-responsive polymers through the in situ co-precipitation process.[26,33,34] Our synthesis utilized a diblock co-polymer of poly(acrylic acid)-block-poly(*N*-isopropylacrylamide) (pAAc-*b*-pNIPAAm), where the deprotonated pAAc block acts as the coordinating segment for the iron cations, whereas the pNIPAAm segment was selected for its water solubility below its lower critical solution temperature (LCST) of 32 °C and aggregation above the LCST.[35] Our new polymer matrix-assisted method enables room-temperature magnetic nanoparticle synthesis with good particle stability and potential for scale-up production. To demonstrate the utility of the new technology, we incorporated the new mNPs into a temperature-responsive binary reagent system separation of protein biomarkers and purification of subpopulations of extracellular vesicles (EVs).

■ RESULTS AND DISCUSSION

Polymer Synthesis and Characterizations.

Temperature-responsive mNPs have been utilized for various biomedical applications, including drug delivery,[36–46] imaging,[47,48] separation and detection.[9,12,49–51] Previous work has shown temperature-responsive iron oxide nanoparticle synthesis using co-precipitation in conjunction with surface modification,[29,52–55] but controlling particle properties, such as diameter and surface functionality, for the intended applications remains a challenge. Here, we have developed a facile straightforward synthesis of temperature-responsive mNPs that utilizes a diblock co-polymer as the template. The resulting iron oxide nanoparticles are

superparamagnetic and temperature responsive without further surface functionalization, and the synthesis is easy and highly reproducible.

The diblock co-polymer, used as the template for particle synthesis, was synthesized according to Scheme 1. The first block of the polymers is composed of NIPAAm, which exhibits a LCST between 30 and 35 °C.[35,56,57] The second block contains AAc, which was designed to complex with iron cations via the carboxylate groups for coordinating the particle synthesis.[26,28,29,34,58] The pNIPAAm was first prepared via reversible addition–fragmentation chain-transfer (RAFT) polymerization of NIPAAm in the presence of the chain-transfer agent (CTA) and a radical initiator. ^{1}H NMR spectroscopy was used to confirm the successful polymerization (Figure S1A).[59] A number average molecular weight (M_n) of 18 820 Da was determined by gel permeation chromatography (GPC) that corresponds to 163 monomeric units of NIPAAm with a polydispersity index (PDI) less than 1.10 (Figure S2). The resultant pNIPAAm block was utilized as the macro CTA (mCTA) for the extension with *tert*-butyl acrylate (*t*-BuA) via RAFT. The chemical shift of *t*-butyl (*t*-Bu) group at 1.4 ppm and the absence of vinyl signals in ^{1}H NMR spectrum (Figure S1B) confirmed the successful addition of *t*-BuA segment.[26] The M_n of the block co-polymer determined by GPC was 20 040 Da corresponding to the addition of 10 *t*-BuA monomeric units with a PDI less than 1.10 (Figure S2). To attain the carboxylates to serve as the coordinating agent with iron cations as previously reported,[26,33,34] the *t*-Bu groups on the polymer were cleaved with 20% trifluoroacetic acid (TFA) in dichloromethane. Complete cleavage of *t*-Bu group was confirmed by the disappearance of the peak at 1.4 ppm in ^{1}H NMR spectrum (Figure S1C).

Magnetic Nanoparticle Synthesis and Characterizations.

The block co-polymer was utilized in the in situ co-precipitation of temperature-responsive iron oxide mNPs (Scheme 2). We tested various particle syntheses by keeping the polymer concentration in the solution constant at 10 mg/ mL (4.99 mM acrylic acid) and varying Fe/COOH ratio from 1.2:1 to 24.2:1 (6.05–120.9 mM) (Table S1). After the addition of NH_4OH for inducing iron oxide formation, all reactions resulted in stable colloids except the reactions with ≥12.1:1 Fe/COOH ratio, which resulted in precipitates immediately. To highlight the importance of the block co-polymer, the same synthesis was carried out either with the pNIPAAm mCTA or without any polymer. Both cases resulted in immediate precipitation of particles, which phase separated from the solutions (Figure S3A,B). Therefore, we conclude that the diblock co-polymer with pAAc segment is essential for synthesizing colloidal stable iron oxide nanoparticles (Figure S3C). The mNPs that are colloidal stable (I-VI) were purified via size exclusion chromatography (SEC) for further characterizations.

The mNPs were characterized by dynamic light scattering (DLS), SEC, and transmission electron microscopy (TEM).[53] The DLS data show that the particle number-averaged diameter increased from 19.8 ± 0.3 to 30.9 ± 0.8 nm when the Fe/COOH ratio varied from 1.2:1 to 9.1:1 during the synthesis (Figure 1A). The corresponding SEC chromato-grams, showing retention time decreasing from 8.88 to 8.17 min, are in good agreement with the DLS analysis. TEM analysis highlights that only the inorganic portion of the particle as

polymers were not stained. The inorganic cores of the particles were predominantly spherical in shape with a broad distribution ranging from approximately 4–24 nm in diameter, as illustrated in Figure S4. The particle separation was evaluated in a simple microtube with a magnetic tube rack. The particles were not aggregated nor captured at room temperature, below the transition temperature. Once the solution temperature was raised to 40 °C, the aggregated particles were captured by the applied magnetic field and the separation efficiencies are summarized in Figure 1B. The separation efficiencies are −10% for particles with Fe/COOH ≤ 3.6:1 (I–III), ~40% for particle with Fe/COOH = 4.8:1 (IV), and nearly 100% for particles with Fe/COOH ≥ 6.5:1 (V and VI). Overall, the syntheses using higher Fe/COOH ratios resulted in particles with larger diameters, which also exhibited higher separation efficiency at 40 °C.

Particle V, which is the smallest particle with nearly 100% separation efficiency, was utilized for additional characterizations. The temperature responsiveness of the particles was ~34 °C, determined by cloud point measurements (Figure S5). The particle solution transitioned from clear to opaque as the particles forming aggregates in response to environment stimuli, such as temperature or pH shift. Measuring the solution absorbance at 500 nm (Figure S5) allowed monitoring the aggregation, which resulted in significant absorbance increase because the aggregates scatter light. The aggregates can be directly observed by eyes and do not exhibit uniform shape nor size. The amount of polymer for temperatureresponsive mNPs was estimated using thermogravimetric analysis (TGA). The analysis shows that ~56 wt % of particle V is polymer (Figure 2). The weight loss at the temperature ≤125 °C is due to residual water in the sample. The percent weight loss from 125 to 600 °C (56% by weight) is attributed to the block co-polymer, which is in agreement with previous studies that indicate the decomposition of pAAc at 260 °C and pNIPAAm from 220 to 440 °c.[60–62]

Stability of Temperature-Responsive mNPs.

Particle stability impacts its potential applications. This work evaluates the stability of the particles, synthesized using the new approach, over a 2 month period by monitoring the particle diameter by DLS, SEC retention time, magnetic separation efficiency, and transition temperature. Both particle V and VI exhibit magnetic separation nearly 100% (Figure 1B) and particle V was chosen for the stability evaluation as it portrays a smaller particle diameter (Figure 1A), which can enable affinity separation with faster kinetics and higher efficiency.[2] The stability evaluation was applied to four particle batches, synthesized using the particle V recipe, Fe/COOH ratio = 6.5:1. After the SEC purification, all particle solutions were kept at room temperature and the particles were analyzed at week 1–4, 6, and 9.

Figure 3A is the particle diameter histogram for batch A at week 1, measured by DLS. The histogram shows the particle diameter varies from 21 to 50 nm with 28.2 nm median. The corresponding histograms for batches B–D can be found in Figure S6. Figure 3B shows the particle diameter distribution over the 2 month period for batch A and the median particle diameter remained ~28 nm, which is similar to the other three batches. The retention time (Figure 4A), analyzed using SEC chromatograms, remained constant around 8.3 min for all four batches over the 2 month period. Additionally, the particle transition temperature

(Figure 4B) stayed constant at 34 °C and the magnetic separation efficiency at 40 °C was ≥95% (Figure 4C) for all four batches over the 2 month period. One solution showed a decrease in magnetic separation at week 4, which was determined to be an outlier as the separation efficiency was restored to >95% after week 4 and remained constant over the following month of analysis. The consistency of the particle size, transition temperature, and magnetic separation proves that these temperature-responsive mNPs can remain stable in solution at room temperature over at least 2 months. TEM images show that the particle's uniformity and dispersibility are not good. However, the particle morphology does not have significant impact for the particle stability. The stability is associated with the polymer surface coverage on the particles as well as the polymer–particle surface interaction. Sufficient coverage keeps particles soluble in aqueous environment, and strong polymer–particle surface interaction keeps the polymers on the particle surface.[29]

Large-Scale Synthesis.

Scalable particle synthesis is essential for commercialization potential. Therefore, the work further challenged particle synthesis scalability by increasing the solution volume to 5×, 10×, and 30×. All syntheses utilized the same recipe as particle V and only modified the solution volumes to 5×, 10×, or 30× accordingly. Figure 5A shows the particle diameter distribution for all three larger scale syntheses, which exhibit median diameter ~28 nm, and the 30× synthesis has slightly wider distribution, 18–50 nm. Additionally, the particle transition temperature (Figure 5B) was ~34 °C. The magnetic separation efficiency at room temperature was ~2% opposed to the separation efficiencies at 40 °C (Figure 5C) were ≥95% for all three larger batch syntheses (Figure S7). These data suggest that the particle synthesis can be utilized for scale-up production.

Temperature-Responsive Binary Reagent System for Affinity Separation.

We have previously developed a binary reagent system for rapid and highly efficient affinity separation of biomolecules.[2,12,63] Compared to the currently utilized magnetic microbead with immobilized antibodies, the binary reagent system comprises two stimuli-responsive reagents, mNPs, constructed with a surface coating of temperature-responsive polymers, and the capture antibody, conjugated to a similar polymer. The key innovation lies in separating the antibody binder from the magnetic particle during the binding step, but bringing them back together upon a small temperature change through the action of the "smart" polymers. Therefore, the diffusive and binding advantages of small nanoscale reagents are exploited. The system comes with the additional advantage of controllable transitions from a stable colloidal suspension to micron-sized aggregates with high magnetophoretic mobility. Our previous work has demonstrated that the binary reagent system exhibits faster and more efficient biomarker isolation when compared to the magnetic microbeads with immobilized antibodies.[2] The temperature-responsive mNPs, synthesized using the new approach, were incorporated into the binary reagent system to demonstrate the separations of proteins and EVs.

Target Protein Analyte Separation.

The protein analyte separation utilized mouse IgG as a model marker. The specimens were prepared by spiking mouse IgG into phosphate-buffered saline (PBS) with 2% bovine serum

albumin (BSA). The temperature-responsive antibody conjugate was synthesized by covalently grafting pNIPAAm to goat anti-mouse IgG using our previous published protocols.[2,12,63] Because the mouse IgG is labeled with Alexa Fluor 488, the separation efficiency can be quantitated by measuring the solution fluorescent intensity after the separation. Decrease of solution fluorescent intensity indicates the mouse IgG removal. The separation data are summarized in Figure 6. Before the separation, the fluorescent intensity for the solution with 12.3 μg/mL mouse IgG was ~2600. After the magnetic separation, the solution fluorescent intensity reduced to ~650 when the conjugate/mouse IgG ratio was 2.2:1. The signal reduced further when the conjugate/mouse IgG ratio was higher. The signal reached bottom when the conjugate/mouse IgG ratio was ≥9:1, which suggests that the separation was maximum. The remaining solution fluorescent signal is likely caused by the denatured mouse IgG and/or free Alexa Fluor 488. Therefore, the temperature-responsive mNPs can be incorporated into the binary reagent system for rapid and efficient protein biomarker separation.

Rapid and Highly Efficient Extracellular Vesicle Separation.

We further evaluated the binary reagent system for extracellular vesicle (EV) separation. To assess EV separation from biological material, we isolated EVs from human semen, which is known to contain a high concentration of EVs that express the common EV tetraspanin markers CD81, CD9, and CD63.[64–66] The EVs were labeled with Dil, a fluorescent lipophilic cationic indocarbocyanine dye to enable detection of EVs in solution before and after separation. The aforementioned anti-mouse IgG conjugates were used in conjunction with monoclonal mouse IgG against human CD81, CD9, and CD63 to enable EV separation; the control experiments utilized a mouse IgG1 χ isotype. Compared to the EV solutions without separation process, the fluorescent intensity of supernatants for the experiments using control and tetraspanin antibodies shows 7 and 25% reductions, respectively (Figure S8). Higher fluorescence reduction indicates EV purification. We also assessed the efficiency of EV purification by quantifying microRNAs known to be carried by EVs from semen. RNA is a biomarker commonly assessed in purified EVs and is likely to be used in many downstream applications of EV separation using this binary reagent system. Analysis of other vesicle content, such as DNA or protein, could be done with alternative lysis protocols. Total RNA was isolated from the positively selected fractions following binary reagent selection for tetraspanin proteins or control IgG. The microRNAs, let-7b and miR-29b, known to be present at high levels in semen EVs,[67,68] were detected by quantitative reverse transcription polymerase chain reaction (PCR) and normalized to the levels of spike-in control (see Experimental Section). Compared to an equivalent volume of untreated EVs or EVs subjected to the isolation protocol using control antibodies, which do not specifically select for EV, let- 7b, and miR-29b were detected at 32- and 178-fold higher concentrations, respectively, in the specifically selected sample (Figure 7). Taken together, these results indicate that the binary reagent system with anti-tetraspanin antibodies selectively isolated EVs. Compared to the Dynabeads, which requires a 2 day separation process, the temperature-responsive binary reagent system isolated EV expressing one or more common tetraspanin markers rapidly in <1.5 h.

CONCLUSIONS

In this study, the diblock co-polymer of pAAc-*b*-pNIPAAm was synthesized by RAFT polymerization. The polymers were later used for the synthesis of superparamagnetic iron oxide mNPs via co-precipitation of iron salts. The new synthesis results in temperature-responsive mNPs in one step without further surface modification. The mNPs reversibly aggregate as the temperature is cycled above and below the transition temperature, 34 °C. Aggregation of the mNPs results in an increase of the effective particle size, facilitating the rapid magnetic separation of the particles by a modest applied field. The new synthesis is a highly reproducible and scalable room-temperature reaction. The resulting particles maintain the same properties and performance for at least 2 months of storage at room temperature. The mNPs can be incorporated into the recently developed temperature-responsive binary reagent system, which decouples the molecular recognition events from the magnetic separation. The binary reagent system enables rapid recognition of target molecule, including proteins and EVs, by the polymer–antibody conjugate in the soluble, hydrophilic state and rapid magnetic separation of the captured molecules after co-aggregation of the conjugates with mNPs. In addition to the biomarker separation, the mNPs can be combined with different affinity reagents as the binary reagent system to enable various applications, including cell manufacturing for enabling immune cell therapy.

EXPERIMENTAL SECTION

Materials.

NIPAAm (Aldrich, 97%) was recrystallized from hexanes and allowed to dry under vacuum prior to use. *tert*-Butyl acrylate (*t*-BuA; Aldrich, 98%) inhibitor was removed by passing through alumina oxide column before use. Hexane (Fisher Scientific, 99.9%), aluminum oxide, activated, basic, Brockmann I, standard grade, ~ 150 mesh, 58 Å (Sigma-Aldrich), 4-Cyano-4-[(dodecylsulfanulthiocarbonyl)sulfanyl]pentanoic acid (DCT; Aldrich, 97%), 4,4′-azobiz(4-cyanovaleric acid) (ACVA; Aldrich, ≥98%), 1,4-dioxane (Fisher Scientific, 99.9%), tetrahydrofuran (THF; Fisher Scientific, 99.9%), ethyl ether anhydrous (Fisher Scientific, 99.9%), pentane (OmniSolv, 98%), trifluoroacetic acid (TFA; Acros, 99%), dichloromethane (EMD, 99.8%), iron(lll) chloride hexahydrate (Sigma-Aldrich, ≥99%), iron(II) chloride tetrahydrate (Sigma-Aldrich, ≥99%), ammonium hydroxide (EDM, 28% as NH_3), boric acid (Fisher Scientific, 99.7%), sodium borate, 10-hydrate (J.T. Baker), *N,N*-dimethylformamide (DMF; BDH, 99%), chloroform-*d*, methanol-d_4 (Cambridge isotope lab), dicyclohexylcarbodiimide, and lithium bromide (Sigma-Aldrich). Phosphate-buffered saline packets (1× PBS; 10 mM phosphate, 138 mM NaCl, 2.7 mM KCl, pH 7.4 at 25 °C) buffers were purchased from Sigma. 4-Cyano-4-(ethylsulfanylthiocarbonyl) sulfanylpentanoic acid (ECT) was synthesized as described previously.[69] Antibodies include goat anti-mouse IgG (Jackson ImmunoResearch, 115–005-008), mouse anti-human CD63 (BD, clone H5C6), mouse anti-human CD81 (R&D Systems, clone 454720), and mouse anti-human CD9 (R&D Systems, clone 209306).

Synthesis.

Poly(N-isopropylacrylamide) Macrochain Transfer Agent.—Polymerization was done via RAFT in 1,4-dioxane. DCT was utilized as the chain-transfer agent (CTA), and ACVA was utilized as the initiator. In the example synthesis, 10.0 g (88.37 mmol) of NIPAAm, 237 mg (0.589 mmol) of DCT, and 16.5 mg (0.0589 mmol) of ACVA were dissolved in 26 mL of 1,4-dioxane in round-bottom flask. The monomer/CTA/initiator ratio was 1500:10:1 to target M_n of 17 kDa. After 30 min of N_2 purging to remove O_2, the flask was placed in an oil bath that has been preheated to 70 °C for 4 h. After cooled to the room temperature, the polymer solution was diluted with THF and purified by precipitating in 12% ethyl ether in pentane. The polymer was dried under vacuum for 24 h.

Poly(acrylic acid)-block-Poly(N-isopropylacrylamide).—The diblock co-polymer of pAAc-*b*-pNIPAAm was synthesized by chain extending mCTA pNIPAAm with *t*-BuA via RAFT and then deprotecting *t*-Bu groups with trifluoroacetic acid to liberate carboxyl groups. The polymerization was performed in 1,4-dioxane with ACVA as the initiator. For a target Mn of 20 kDa, the monomer/mCTA/ initiator molar ratio was 199:9:1. In the example synthesis, 7.0 g of mCTA (0.372 mmol), 1.03 g (8.07 mmol) of *t*-BuA, 11.3 mg (40.3 μmol) of ACVA were dissolved in 32 mL of 1,4-dioxane in round- bottom flask. After 30 min of N_2 purging to remove O_2, the flask was placed in an oil bath that has been preheated to 70 °C for 5 h. After cooled to the room temperature, the polymer solution was diluted with THF and purified by precipitating in 12% ethyl ether in pentane. The polymer was dried under vacuum for 24 h.

The deprotection was carried out by treating ptBuA-*b*-pNIPAAm with 20% TFA in dichloromethane for 4 h at room temperature. After removing dichloromethane via rotary evaporation, the solution was precipitated in 12% ethyl ether in pentane for purification. The polymer was further purified via two additional washes with ethyl ether and pentane mixture and dried under vacuum.

Poly(N-isopropylacrylamide) with an End N-Hydroxysuccinimide (NHS) Ester.—The synthesis of pNIPAAm-NHS is a two-step process, containing the synthesis of pNIPAAm and the conversion of carboxylate to an active ester. Polymerization was done via RAFT in 1,4-dioxane. ECT was utilized as the CTA, and ACVA was utilized as the initiator. In the example synthesis, 4.97 g, (43.9 mmol) of NIPAAm, 32.6 mg (0.120 mmol) of ECT, and 3.5 mg (0.01 mmol) of ACVA were dissolved in 12.5 mL of 1,4-dioxane in round-bottom flask. After 30 min of N_2 purging to remove O_2, the flask was placed in an oil bath that has been preheated to 70 °C for 4 h. The polymers were collected by precipitation into 90% pentane/10% ether followed by vacuum-drying. To produce an amine-reactive NHS ester (pNIPAAm-NHS), pNIPAAm (2.5 g) and NHS (0.016 g) were dissolved in 10 mL of dichloromethane. Dicyclohexylcarbodiimide (0.029 g) was added to this solution, and the reaction was stirred at room temperature for 24 h. The polymer was collected by precipitation into pentane and dried in vacuo.

Temperature-Responsive Iron Oxide Magnetic Nanoparticles.

The particles were synthesized via co-precipitation with pAAc-*b*-pNIPAAm as the template. The polymer was predissolved in nanopure H2O at 50 mg/mL. $FeCl_2$ and $FeCl_3$ were predissolved in nanopure H_2O at 0.065 M with the $FeCl_2/FeCl_3$ molar ratio as 1:2. The polymer solution, iron salt solution, and additional nanopure H_2O were purged with N_2 to remove O_2. For 1 mL synthesis, 200 μL of polymer solution was mixed with 300 μL of nanopure H2O and 500 μL of iron salt solution. After stirring for 30 min, 40 μL of NH_4OH (28% NH_3 in H_2O) was added into the mixture. The solution changed from clear transparent to light brown. After 30 min at room temperature, the solution was filtered with 0.2 μm poly(vinylidene difluoride) (PVDF) syringe filter. The mNPs in the filtrate were purified via size exclusion chromatography (SEC) performed on BioCAD SPRINT Workstation, equipped with BioSEP-SEC-s4000 column made by Phenomenex. The mobile phase was 20 mM borate buffer at a flow rate of 5 mL/min with absorbance measured at 306 nm. The SEC-purified particles were concentrated with a 30 kDa Amicon Ultra Centrifugal filter. After purification, the particles were collected by lyophilization.

Polymer–Antibody Conjugate.—The conjugates were prepared by mixing pNIPAAm-NHS and antibodies (Abs) at a polymer/antibody molar ratio of 100:1. Goat anti-mouse IgG, Fc γ fragment specific, was diluted into 25 mM $Na_2CO_3/NaHCO_3$, pH 9.5, and cooled. The pNIPAM-NHS was added to the Ab solution and mixed for 18 h at 4 °C. The solution was filtered with 0.2 μm PVDF syringe filter. The conjugates in the filtrate were isolated via size exclusion chromatography (SEC), which was used for mNP purification. The SEC-purified conjugates were concentrated with a 30 kDa Amicon Ultra Centrifugal filter.

Characterizations.

Gel Permeation Chromatography.—Polymer molecular weights and polydispersity were characterized by gel permeation chromatography. Columns utilized were Tosoh SEC TSK-GEL α−3000 and α-e4000 (Tosoh Bioscience, Montgomeryville, PA). They were attached to Agilent 1200 Series Liquid Chromatography System (Santa Clara, CA), Wyatt Technology miniDAWN TREOS, 3 angle MALS light scattering instrument, and Optilab T-rEX, refractive index (RI) detector (Santa Barbara, CA). The mobile phase flow rate was 1 mL/min at 60 °C, which consists of 0.1 wt % LiBr in high-performance liquid chromatography-grade DMF. The *dn/dc* value for polymers was determined by making polymer concentrations of: 0.5, 1.0, 1.5, 2.0, 2.5, 3.0 mg/mL, which were analyzed by the RI detector postcolumn.

^{1}H NMR Analysis.—The chemical composition of mCTA was confirmed by ^{1}H NMR spectrum (300 MHz, $CDCl_3$, δ (ppm): 4.00, 1.16 (s, R− CO−NH−C<u>H</u>−$(CH_3)_2$)). Chemical composition for ptBuA-*b*-pNIPAAm was confirmed ^{1}H NMR spectrum (300 MHz, $CDCl_3$, δ (ppm): 4.0, 1.16 (s, R−CO−NH−C<u>H</u>−$(CH_3)_2$), 1.4 (s, R−CO−O($\underline{H}_3$)$_3$). Complete cleavage of *tert*-butyl group yielding p(NIPAAm)-*b*-p(acrylic acid) was confirmed by ^{1}H NMR spectrum (300 MHz, MeOD) showing the absence of peak at δ 1.4 ppm (s, R−CO−O(C<u>H</u>$_3$)$_3$) corresponding to *t*-butyl group. The protons corresponding to methylene and methane on the main chain have peaks at δ 1.60, 2.10 ppm, respectively, for all polymers.

Dynamic Light Scattering.—Hydrodynamic diameter measurements were taken with Zetasizer Nano ZS instrument. A 633 nm He−Ne laser was utilized as the incident beam, and the measurements were performed at 173° backscatter angle. 1 mL samples of 1.22 mg/mL mNPs in PBS, filtered by 0.2 μm cutoff PVDF filters were used for the particle size measurements. A minimum of three measurements was taken for each sample.

Size Exclusion Chromatography.—The mNPs were injected into the BioCAD SPRINT Workstation equipped with BioSEP-SEC-s4000 column made by Phenomenex. Samples were injected into 2 mL of loop at 0.30 mg/mL concentration. The retention time was defined as the time at which the peak height attains the maximum in the chromatogram.

Transmission Electron Microscopy.—The morphology for the magnetic nanoparticles was analyzed utilizing a Tecnai G2 F20 Superwin transmission electron microscope (200 kV). The colloidal solution of mNPs in water was deposited onto 300 mesh lacy carbon on copper grid as well as 300 mesh single layer grapheme on lacy carbon grid both made by Ted Pella and allowed to dry before analysis. The images were analyzed via ImageJ, to measure the diameter of the particles.

Magnetic Separation Efficiency.—To characterize magnetic separation efficiency, 180 μL of 1.22 mg/mL mNP solution in PBS was taken in 1.5 mL microfuge tube and incubated at 40 °C for 3 min. Subsequently, the tube was transferred to a magnetic heatblock at 40 °C and allowed to separate for 3 min. The supernatant was collected and analyzed using the spectrophotometer, Hewlett Packard 8452A diode array. The supernatant was compared to the mNP solution before the separation using absorbance at 450 nm to determine the separation efficiency as follows

$$\% \text{ separation } = \frac{A_{450_b} - A_{450_s}}{A_{450_b}} \times 100\% \quad (1)$$

$A_{.450b}$ and $A_{.450s}$ are the absorbance at 450 nm for the solution before magnetic separation and the supernatant. For room-temperature separation, the same procedure was followed, however, particles were incubated at 25 °C instead of 40 °C.

Thermogravimetric Analysis.—A total of 5 mg of mNP was utilized to determine the amount of polymer that coordinated with iron oxide surfaces. The measurements were carried out on PerkinElmer TGA—Pyris 7 instrument under nitrogen, from 30 to 600 °C at a heating rate of 10 °C/min.

Cloud Point Measurement.—The transition temperature was identified as the temperature at which the absorbance at 500 nm reached 0.5 au. The concentration of mNPs was 1.22 mg/mL in PBS. The data were collected using a UV–vis spectrophotometer with a jacketed cuvette holder to control the temperature of the sample. A heating rate of 0.5 °C/min was used, and absorbance values were measured every 0.5–1.0 °C.

Separation via the Binary Reagent System.

Mouse IgG Separation.—The protein analyte separation utilized mouse IgG as the model marker. The specimens were prepared by spiking mouse IgG into PBS with 2% BSA. The total volume for each experiment was 122 μL, containing 60 μL of mouse IgG (25 μg/mL), 12.2 μL of mNPs (12 mg/mL), and various amount of anti-mouse IgG polymer–antibody conjugates. After the addition of conjugates and mNPs, the solution mixer was briefly vortexed. Then, followed the aforementioned magnetic separation protocol to isolate the analytes. After the separation, the supernatants were collected for fluorescence measurement to determine the separation efficiency.

Extracellular Vesicle Separation.—The separation utilized EVs from semen. All semen samples were obtained from healthy men volunteering for research studies at the University of Washington. Protocols were approved by the institutional review boards of the University of Washington. Ejaculates were collected in sterile containers and frozen at –20 °C prior to processing. EVs were purified as described,[67] briefly, semen samples were allowed to thaw and liquefy for 20 min at room temperature. Seminal plasma, containing exosomes, was separated from the cell fraction and cell debris by centrifugation at 1000g for 10 min, then centrifugation at 2400g for 30 min followed by 0.45 and 0.22 μm syringe filtration (Millex HA). EVs were purified by ultracentrifugation at 100 000g for 90 min at over a sucrose cushion composed of a 20 mM Tris/30% sucrose/deuterium oxide (D_2O) cushion (pH 7.4) (Sigma). The upper layer was collected and ultracentrifuged again at 100 000g for 14 h at 4 °C over a 20 mM Tris/25% sucrose/D_2O cushion (pH 7.4). The 30 and 25% sucrose cushions containing the EV fraction were pooled and washed with 30 mL of PBS by centrifuging at 2400g through an Amicon Ultracel 100 kDa cellulose centrifugal filter and concentrated to a final volume of 425 μL to 3.2 mL. EVs were stored at −80 °C. All experiments used pools of EVs from five individual men.

To monitor the EV separation via fluorescence measurement, semen EV pools were stained with DiI lipophilic tracer at 0.5 mg/mL for 20 min at 37 °C according to manufacturer's instructions (Thermo Fisher). After staining, SEV were resuspended in 15 mL of PBS and washed and concentrated to their original volume by centrifugation at 2400g in an Amicon Ultracel 100 kDa cellulose centrifugal filter.

For EV separation, the total volume for each experiment was 400 μL, including 200μL of purified Dil labeled EVs, 10μL of tetraspanin (or control) antibodies, 40 μL of 250 mM NaCl, and 40 μL of mNPs. The rest of volume was filled up with PBS. Each experiment contained 5 μg (33.3 pmol) of mouse anti-human tetraspanin (or control) antibodies, 160 pmol anti-mouse IgG conjugates, 10 μmol NaCl, and 400 μg mNPs. The tetraspanin antibodies included equal amount of mouse IgG antibodies against human CD63, CD9, and CD81, and the control experiments used a mouse IgG1 χ isotype. After the addition of tetraspanin (or control) antibodies, the solution mixers were incubated for 30 min. The same incubation was applied to the solution mixer after the addition of the anti-mouse IgG conjugates. Then, the mixtures were incubated at 40 °C for 5 min before magnetic separation at 40 °C for 5 min. The supernatants were collected for fluorescence measurement, and the captured pellets were collected for RNA analysis.

For RNA extraction, 5 μL of 5 nM synthetic cel-miR-39 (Qiagen) was added to EV purified with binary reagent system during lysis to normalize RNA extraction and reverse transcription across samples. Total RNA was isolated using the miRCURY RNA Isolation kit (Exiqon) according to the manufacturer's instructions. Reverse transcription was carried out using specific primers for cel-miR-39, mir-29b, and let-7b using Taqman microRNA reverse transcription kits according to instructions (Thermo Fisher). After reverse transcription, cDNA was diluted fivefold with water and 6.75 μL of cDNA was used in a 15 μL final PCR reaction volume using Taqman 2× master mix and Taqman microRNA primer/probe sets, according to instructions (Thermo Fisher).

Supplementary Material

Refer to Web version on PubMed Central for supplementary material.

■ ACKNOWLEDGMENTS

The authors thank Dr. Anthony Convertine for assisting polymer characterization via GPC and Dr. Fang-Yi Su for assisting particle characterization via TEM.

Funding

Funds used to support the research of the manuscript were provided by NIH, including GM086304, CA174581, HD089679, DA040386, and AI129303.

■ REFERENCES

(1). Fang X; Zhang W-W Affinity Separation and Enrichment Methods in Proteomic Analysis. J. Proteomics 2008, 71, 284–303. [PubMed: 18619565]

(2). Nehilla BJ; Hill JJ; Srinivasan S; Chen Y-C; Schulte TH; Stayton PS; Lai JJ A Stimuli-Responsive, Binary Reagent System for Rapid Isolation of Protein Biomarkers. Anal. Chem. 2016, 88, 10404–10410. [PubMed: 27686335]

(3). Sheng S; Kong F Separation of Antigens and Antibodies by Immunoaffinity Chromatography. Pharm. Biol. 2012, 1038–1044. [PubMed: 22480305]

(4). Berna MJ; Zhen Y; Watson DE; Hale JE; Ackermann BL Strategic Use of Immunoprecipitation and LC/MS/MS for Trace-Level Protein Quantification: Myosin Light Chain 1, a Biomarker of Cardiac Necrosis. Anal. Chem. 2007, 79, 4199–4205. [PubMed: 17447729]

(5). Whiteaker JR; Zhao L; Zhang HY; Feng L-C; Piening BD; Anderson L; Paulovich AG Antibody-Based Enrichment of Peptides on Magnetic Beads for Mass-Spectrometry-Based Quantification of Serum Biomarkers. Anal. Biochem. 2007, 362, 44–54. [PubMed: 17241609]

(6). Niemeyer CM Nanoparticles, Proteins, and Nucleic Acids: Biotechnology Meets Materials Science. Angew. Chem., Int. Ed. 2001, 40, 4128–4158.

(7). McCloskey KE; Chalmers JJ; Zborowski M Magnetophoretic Mobilities Correlate to Antibody Binding Capacities. Cytometry 2000, 40, 307–315. [PubMed: 10918281]

(8). Moore LR; Zborowski M; Sun L; Chalmers JJ Lymphocyte Fractionation Using Immunomagnetic Colloid and a Dipole Magnet Flow Cell Sorter. J. Biochem. Biophys. Methods 1998, 37, 11–33. [PubMed: 9825297]

(9). Lai JJ; Hoffman JM; Ebara M; Hoffman AS; Estournes C; Wattiaux A; Stayton PS Dual Magnetic-/Temperature-Responsive Nanoparticles for Microfluidic Separations and Assays. Langmuir 2007, 23, 7385–7391. [PubMed: 17503854]

(10). Lai JJ; Nelson KE; Nash MA; Hoffman AS; Yager P; Stayton PS Dynamic Bioprocessing and Microfluidic Transport Control with Smart Magnetic Nanoparticles in Laminar-Flow Devices. Lab Chip 2009, 9, 1997–2002. [PubMed: 19568666]

(11). Nash MA; Lai JJ; Hoffman AS; Yager P; Stayton PS “Smart” Diblock Copolymers as Templates for Magnetic-Core GoldShell Nanoparticle Synthesis. Nano Lett. 2010, 10, 85–91. [PubMed: 20017498]

(12). Phan JC; Nehilla BJ; Srinivasan S; Coombs RW; Woodrow KA; Lai JJ Human Immunodeficiency Virus (HIV) Separation and Enrichment via the Combination of Antiviral Lectin Recognition and a Thermoresponsive Reagent System. Pharm. Res. 2016, 33, 2411–2420. [PubMed: 27401412]

(13). Furukawa H; Shimojyo R; Ohnishi N; Fukuda H; Kondo A Affinity Selection of Target Cells from Cell Surface Displayed Libraries: A Novel Procedure Using Thermo-Responsive Magnetic Nanoparticles. Appl. Microbiol. Biotechnol 2003, 62, 478–483. [PubMed: 12750854]

(14). Fukuda N; Ishii J; Tanaka T; Fukuda H; Ohnishi N; Kondo A Rapid and Efficient Selection of Yeast Displaying a Target Protein Using Thermo-Responsive Magnetic Nanoparticles. Biotechnol. Prog. 2008, 24, 352–357. [PubMed: 18324826]

(15). Majewski AP; Schallon A; Jerome V; Freitag R; Muller AH; Schmalz H Dual-Responsive Magnetic Core-Shell Nanoparticles for Nonviral Gene Delivery and Cell Separation. Biomacromolecules 2012, 13, 857–866. [PubMed: 22296556]

(16). Peng H; Luo M; Xiong H; Yu N; Ning F; Fan J; Zeng Z; Li J; Chen L Preparation of Photonic-Magnetic Responsive Molecularly Imprinted Microspheres and Their Application to Fast and Selective Extraction of 17β-Estradiol. J. Chromatogr. A 2016, 1442, 1–11. [PubMed: 27000739]

(17). Massart R Preparation of Aqueous Magnetic Liquids in Alkaline and Acidic Media. IEEE Trans. Magn. 1981, 17, 1247–1248.

(18). Woo K; Hong J; Choi S; Lee H-W; Ahn J-P; Kim CS; Lee SW Easy Synthesis and Magnetic Properties of Iron Oxide Nanoparticles. Chem. Mater. 2004, 16, 2814–2818.

(19). Ge S; Shi X; Sun K; Li C; Uher C; Baker JR Jr.; Holl MMB; Orr BG Facile Hydrothermal Synthesis of Iron Oxide Nanoparticles with Tunable Magnetic Properties. J. Phys. Chem. C 2009, 113, 13593–13599.

(20). Hou Y; Yu J; Gao S Solvothermal Reduction Synthesis and Characterization of Superparamagnetic Magnetite Nanoparticles. J. Mater. Chem. 2003, 13, 1983–1987.

(21). Xu J; Yang H; Fu W; Du K; Sui Y; Chen J; Zeng Y; Li M; Zou G Preparation and Magnetic Properties of Magnetite Nanoparticles by Sol-Gel Method. J. Magn. Magn. Mater. 2007, 309, 307–311.

(22). Caruntu D; Caruntu G; O’Connor CJ Magnetic Properties of Variable-Sized Fe_3O_4 Nanoparticles Synthesized from Non-Aqueous Homogeneous Solutions of Polyols. J. Phys. D: Appl. Phys. 2007, 40, 5801.

(23). Darbandi M; Stromberg F; Landers J; Reckers N; Sanyal B; Keune W; Wende H Nanoscale Size Effect on Surface Spin Canting in Iron Oxide Nanoparticles Synthesized by the Microemulsion Method. J. Phys. D: Appl. Phys. 2012, 45, No. 195001.

(24). Theerdhala S; Bahadur D; Vitta S; Perkas N; Zhong Z; Gedanken A Sonochemical Stabilization of Ultrafine Colloidal Biocompatible Magnetite Nanoparticles Using Amino Acid, LArginine, for Possible Bio Applications. Ultrason. Sonochem. 2010, 17, 730–737. [PubMed: 20042358]

(25). Sreeja V; Joy P Microwave-Hydrothermal Synthesis of r- Fe_2O_3 Nanoparticles and Their Magnetic Properties. Mater. Res. Bull. 2007, 42, 1570–1576.

(26). Basuki JS; Jacquemin A; Esser L; Li Y; Boyer C; Davis TP A Block Copolymer-Stabilized Co-Precipitation Approach to Magnetic Iron Oxide Nanoparticles for Potential Use as Mri Contrast Agents. Polym. Chem. 2014, 5, 2611–2620.

(27). Wakamatsu H; Yamamoto K; Nakao A; Aoyagi T Preparation and Characterization of Temperature-Responsive Magnetite Nanoparticles Conjugated with N-Isopropylacrylamide-Based Functional Copolymer. J. Magn. Magn. Mater. 2006, 302, 327–333.

(28). Bakandritsos A; Papagiannopoulos A; Anagnostou EN; Avgoustakis K; Zboril R; Pispas S; Tucek J; Ryukhtin V; Bouropoulos N; Kolokithas-Ntoukas A; et al. Merging High Doxorubicin Loading with Pronounced Magnetic Response and Bio-Repellent Properties in Hybrid Drug Nanocarriers. Small 2012, 8, 2381–2393. [PubMed: 22549909]

(29). Jiang X; Zhai S; Jiang X; Lu G; Huang X Synthesis of PAA-G-PNIPAM Well-Defined Graft Polymer by Sequential RAFT and SET-LRP and Its Application in Preparing Size-Controlled Super-Paramagnetic Fe_3O_4 Nanoparticles as a Stabilizer. Polymer 2014, 55, 3703–3712.

(30). Shamim N; Hong L; Hidajat K; Uddin M Thermosensitive Polymer (N-Isopropylacrylamide) Coated Nanomagnetic Particles: Preparation and Characterization. Colloids Surf. B 2007, 55, 51–58.

(31). Wang H; Luo W; Chen J Fabrication and Characterization of Thermoresponsive Fe_3O_4@PNIPAM Hybrid Nanomaterials by Surface-Initiated RAFT Polymerization. J. Mater. Sci 2012, 47, 5918–5925.

(32). Aqil A; Vasseur S; Duguet E; Passirani C; Benoît J-P; Jérôme R; Jérôme C Magnetic Nanoparticles Coated by Temperature Responsive Copolymers for Hyperthermia. J. Mater. Chem. 2008, 18, 3352–3360.

(33). Lutz JF; Stiller S; Hoth A; Kaufner L; Pison U; Cartier R One-Pot Synthesis of Pegylated Ultrasmall Iron-Oxide Nanoparticles and Their in Vivo Evaluation as Magnetic Resonance Imaging Contrast Agents. Biomacromolecules 2006, 7, 3132–3138. [PubMed: 17096542]

(34). Si S; Kotal A; Mandal TK; Giri S; Nakamura H; Kohara T Size-Controlled Synthesis of Magnetite Nanoparticles in the Presence of Polyelectrolytes. Chem. Mater. 2004, 16, 3489–3496.

(35). Heskins M; Guillet JE Solution Properties of Poly(N-Isopropylacrylamide). J. Macromol. Sci., Chem. 1968, 2, 1441–1455.

(36). Kaamyabi S; Badrian A; Akbarzadeh A Synthesis of Cross-Linked Poly(N-Isopropylacrylamide) Magnetic Nano Composite for Application in the Controlled Release of Doxorubicin. Pharm. Nanotechnol 2017, 5, 67–75. [PubMed: 28948911]

(37). Jamal Al Dine E.; Ferjaoui Z; Ghanbaja J; Roques-Carmes T; Meftah A; Hamieh T; Toufaily J; Schneider R; Marchal S; Gaffet E; Alem H Thermo-Responsive Magnetic Fe3O4@P-(MEO2MAx-OEGMA100-x) NPs and Their Applications as Drug Delivery Systems. Int. J. Pharm. 2017, 532, 738–747. [PubMed: 28893585]

(38). Shen B; Ma Y; Yu S; Ji C Smart Multifunctional Magnetic Nanoparticle-Based Drug Delivery System for Cancer Thermo-Chemotherapy and Intracellular Imaging. ACS Appl. Mater. Interfaces 2016, 8, 24502–24508. [PubMed: 27573061]

(39). Jaiswal MK; Pradhan A; Banerjee R; Bahadur D Dual pH and Temperature Stimuli-Responsive Magnetic Nanohydrogels for Thermo-Chemotherapy. J. Nanosci. Nanotechnol. 2014, 14, 4082–4089. [PubMed: 24738355]

(40). Wang Y; Wu G; Li X; Wang Y; Gao H; Ma J Synthesis, Characterization and Controlled Drug Release from Temperature-Responsive Poly(Ether-Urethane) Particles Based on PEG-Diisocyanates and Aliphatic Diols. J. Biomater. Sci., Polym. Ed. 2013, 24, 1676–1691. [PubMed: 23627737]

(41). Wang N; Guan Y; Yang L; Jia L; Wei X; Liu H; Guo C Magnetic Nanoparticles (MNPs) Covalently Coated by PEO-PPO-PEO Block Copolymer for Drug Delivery. J. Colloid Interface Sci. 2013, 395, 50–57. [PubMed: 23305884]

(42). Wang A; Gao H; Sun Y; Sun YL; Yang YW; Wu G; Wang Y; Fan Y; Ma J Temperature- and pH-Responsive Nanoparticles of Biocompatible Polyurethanes for Doxorubicin Delivery. Int. J. Pharm. 2013, 441, 30–39. [PubMed: 23262421]

(43). Koppolu B; Bhavsar Z; Wadajkar AS; Nattama S; Rahimi M; Nwariaku F; Nguyen KT Temperature-Sensitive Polymer-Coated Magnetic Nanoparticles as a Potential Drug Delivery System for Targeted Therapy of Thyroid Cancer. J. Biomed. Nanotechnol. 2012, 8, 983–990. [PubMed: 23030006]

(44). Dehvari K; Lin KS Synthesis, Characterization and Potential Applications of Multifunctional PEO-PPOPEO-Magnetic Drug Delivery System. Curr. Med. Chem. 2012, 19, 5199–5204. [PubMed: 23237189]

(45). Yao A; Chen Q; Ai F; Wang D; Huang W Preparation and Characterization of Temperature-Responsive Magnetic Composite Particles for Multi-Modal Cancer Therapy. J. Mater. Sci.: Mater. Med. 2011, 22, 2239–2247. [PubMed: 21833605]

(46). Deka SR; Quarta A; Di Corato R; Riedinger A; Cingolani R; Pellegrino T Magnetic Nanobeads Decorated by Thermo-Responsive PNIPAM Shell as Medical Platforms for the Efficient Delivery of Doxorubicin to Tumour Cells. Nanoscale 2011, 3, 619–629. [PubMed: 21082085]

(47). Shuhendler AJ; Staruch R; Oakden W; Gordijo CR; Rauth AM; Stanisz GJ; Chopra R; Wu XY Thermally- Triggered 'Off-on-Off Response of Gadolinium-Hydrogel-Lipid Hybrid Nanoparticles Defines a Customizable Temperature Window for Non-Invasive Magnetic Resonance Imaging Thermometry. J. Controlled Release 2012, 157, 478–484.

(48). Hannecart A; Stanicki D; Vander Elst L; Muller RN; Lecommandoux S; Thevenot J; Bonduelle C; Trotier A; Massot P; Miraux S; Sandre O; Laurent S Nano-Thermometers with Thermo-Sensitive Polymer Grafted USPIOs Behaving as Positive Contrast Agents in Low-Field MRI. Nanoscale 2015, 7, 3754–3767. [PubMed: 25644780]

(49). Oh S; Kim J; Tran VT; Lee DK; Ahmed SR; Hong JC; Lee J; Park EY; Lee J Magnetic Nanozyme-Linked Immunosorbent Assay for Ultrasensitive Influenza a Virus Detection. ACS Appl. Mater. Interfaces 2018, 10, 12534–12543.

(50). Chen Y; Xianyu Y; Wang Y; Zhang X; Cha R; Sun J; Jiang X One-Step Detection of Pathogens and Viruses: Combining Magnetic Relaxation Switching and Magnetic Separation. ACS Nano 2015, 9, 3184–3191. [PubMed: 25743636]

(51). Chen H-W; Fang Z-S; Chen Y-T; Chen Y-I; Yao B-Y; Cheng J-Y; Chien C-Y; Chang Y-C; Hu C-MJ Targeting and Enrichment of Viral Pathogen by Cell Membrane Cloaked Magnetic Nanoparticles for Enhanced Detection. ACS Appl. Mater. Interfaces 2017, 9, 39953–39961. [PubMed: 29088538]

(52). Narain R; Gonzales M; Hoffman AS; Stayton PS; Krishnan KM Synthesis of Monodisperse Biotinylated P-(NIPAAM)-Coated Iron Oxide Magnetic Nanoparticles and Their Bioconjugation to Streptavidin. Langmuir 2007, 23, 6299–6304. [PubMed: 17451262]

(53). Heidarinasab A; Panahi HA; Faramarzi M; Farjadian F Synthesis of Thermosensitive Magnetic Nanocarrier for Controlled Sorafenib Delivery. Mater. Sci. Eng. C 2016, 67, 42–50.

(54). Moazen MK; Panahi HA Magnetic Iron Oxide Nanoparticles Grafted N-Isopropylacrylamide/ Chitosan Copolymer for the Extraction and Determination of Letrozole in Human Biological Samples. J. Sep. Sci. 2017, 40, 1125–1132. [PubMed: 28052589]

(55). Shamim N; Hong L; Hidajat K; Uddin M Thermosensitive-Polymer-Coated Magnetic Nanoparticles: Adsorption and Desorption of Bovine Serum Albumin. J. Colloid Interface Sci. 2006, 304, 1–8. [PubMed: 17010360]

(56). Schild HG Poly(N-Isopropylacrylamide): Experiment, Theory and Application. Prog. Polym. Sci. 1992, 17, 163–249.

(57). Liu R; Fraylich M; Saunders BR Thermoresponsive Copolymers: From Fundamental Studies to Applications. Colloid Polym. Sci. 2009, 287, 627–643.

(58). Lutz J-F; Stiller S; Hoth A; Kaufner L; Pison U; Cartier R One-Pot Synthesis of Pegylated Ultrasmall Iron-Oxide Nanoparticles and Their in Vivo Evaluation as Magnetic Resonance Imaging Contrast Agents. Biomacromolecules 2006, 7, 3132–3138. [PubMed: 17096542]

(59). Illescas J; Casu M; Alzari V; Nuvoli D; Scorciapino MA; Sanna R; Sanna V; Mariani A Poly(Ionic Liquid)s Derived from 3-Octyl-1-Vinylimidazolium Bromide and N-Isopropylacrylamide with Tunable Properties. J. Polym. Sci., Part A: Polym. Chem. 2014, 52, 3521–3532.

(60). Schild HG Thermal Decomposition of PNIPAAM: TGA-FTIR Analysis. J. Polym. Sci. Part A: Polym. Chem. 1996, 34, 2259–2262.

(61). Liao MH; Chen DH Preparation and Characterization of a Novel Magnetic Nano-Adsorbent. J. Mater. Chem. 2002, 12, 3654–3659.

(62). Wang HD; Luo WQ; Chen JC Fabrication and Characterization of Thermoresponsive Fe_3O_4@PNIPAM Hybrid Nanomaterials by Surface-Initiated RAFT Polymerization. J. Mater. Sci. 2012, 47, 5918–5925.

(63). Roy D; Nehilla BJ; Lai JJ; Stayton PS Stimuli-Responsive Polymer-Antibody Conjugates Via RAFT and Tetrafluorophenyl Active Ester Chemistry. ACS Macro Lett. 2013, 2, 132–136.

(64). Poliakov A; Spilman M; Dokland T; Amling CL; Mobley JA Structural Heterogeneity and Protein Composition of Exosome- Like Vesicles (Prostasomes) in Human Semen. Prostate 2009, 69, 159–167. [PubMed: 18819103]

(65). Utleg AG; Yi EC; Xie T; Shannon P; White JT; Goodlett DR; Hood L; Lin B Proteomic Analysis of Human Prostasomes. Prostate 2003, 56, 150–161. [PubMed: 12746840]

(66). Lötvall J; Hill AF; Hochberg F; Buzás EI; Di Vizio D; Gardiner C; Gho YS; Kurochkin IV; Mathivanan S; Quesenberry P; Sahoo S; Tahara H; Wauben MH; Witwer KW; Théry C Minimal Experimental Requirements for Definition of Extracellular Vesicles and Their Functions: A Position Statement from the International Society for Extracellular Vesicles. J. Extracell. Vesicles 2014, 3, 26913. [PubMed: 25536934]

(67). Vojtech L; Woo S; Hughes S; Levy C; Ballweber L; Sauteraud RP; Strobl J; Westerberg K; Gottardo R; Tewari M; Hladik F Exosomes in Human Semen Carry a Distinctive Repertoire of Small Non-Coding RNAs with Potential Regulatory Functions. Nucleic Acids Res. 2014, 42, 7290–7304. [PubMed: 24838567]

(68). Chevillet JR; Kang Q; Ruf IK; Briggs HA; Vojtech LN; Hughes SM; Cheng HH; Arroyo JD; Meredith EK; Gallichotte EN; Pogosova-Agadjanyan EL; Morrissey C; Stirewalt DL; Hladik F; Yu EY; Higano CS; Tewari M Quantitative and Stoichiometric Analysis of the Microrna Content of Exosomes. Proc. Natl. Acad. Sci. U.S.A. 2014, 111, 14888–14893. [PubMed: 25267620]

(69). Convertine AJ; Benoit DS; Duvall CL; Hoffman AS; Stayton PS Development of a Novel Endosomolytic Diblock Copolymer for Sirna Delivery. J. Controlled Release 2009, 133, 221–229.

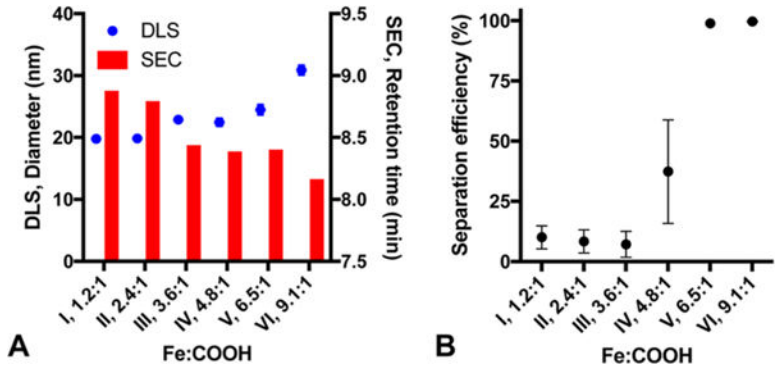

Figure 1.

Characterizations of temperature-responsive mNPs. (A) Dynamic light scattering (DLS) analysis shows the particle diameter varied from 19.8 ± 0.3 to 30.9 ± 0.8 nm when the Fe/COOH ratio varied from 1.2:1 to 9.1:1 during the synthesis. The SEC analysis shows the decrease of retention time from 8.88 to 8.17 min. Shorter retention time for higher Fe/COOH ratio indicates larger particle diameter, which is in good agreement with the DLS analysis. (B) The mNP separation at 40 °C. The separation efficiencies were ≤10% for the particles with smaller diameter (Fe/COOH ≤ 3.6:1), increased to ~40% for the particle with slightly larger diameter (Fe/COOH = 4.8:1), and further increased to nearly 100% for the two larger particles (Fe/COOH ≥ 6.5:1).

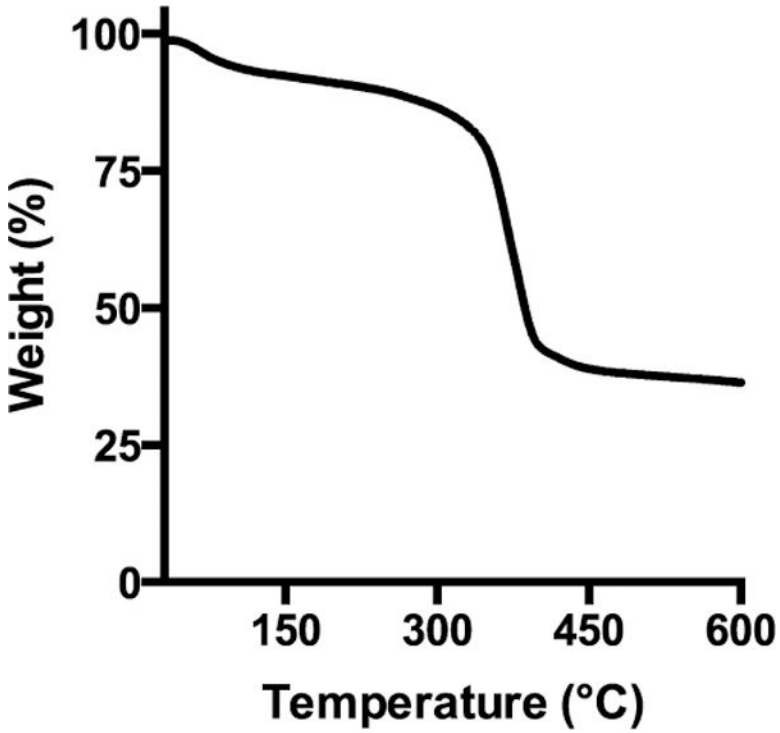

Figure 2.

Thermogravimetric analysis (TGA) curve shows weight loss at the temperature ≤125 °C, which is likely due to residual water in the sample. The weight loss from 125 to 600 °C is attributed to the polymer, which is ~56% of the particle mass.

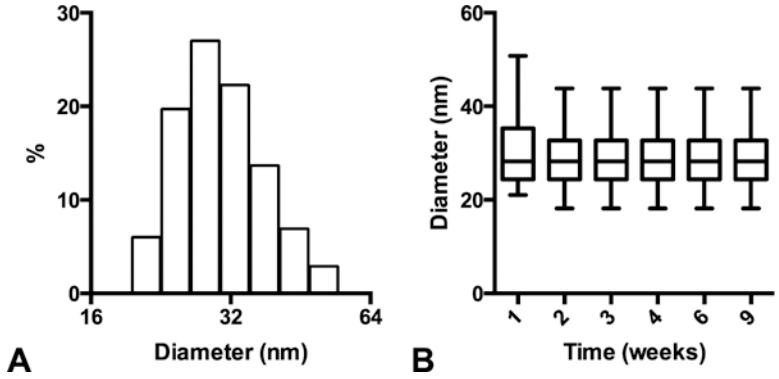

Figure 3.

DLS analysis for particle size distribution. (A) Particle size distribution right after the synthesis shows that the particle diameter varies from 21 to 50 nm with 28.2 nm median. (B) The monitoring of particle size distribution over a 2 month storage at room temperature shows that the particle diameters were slightly smaller but not statistically significantly different when compared to week 1. The median particle diameter remained ~28 nm.

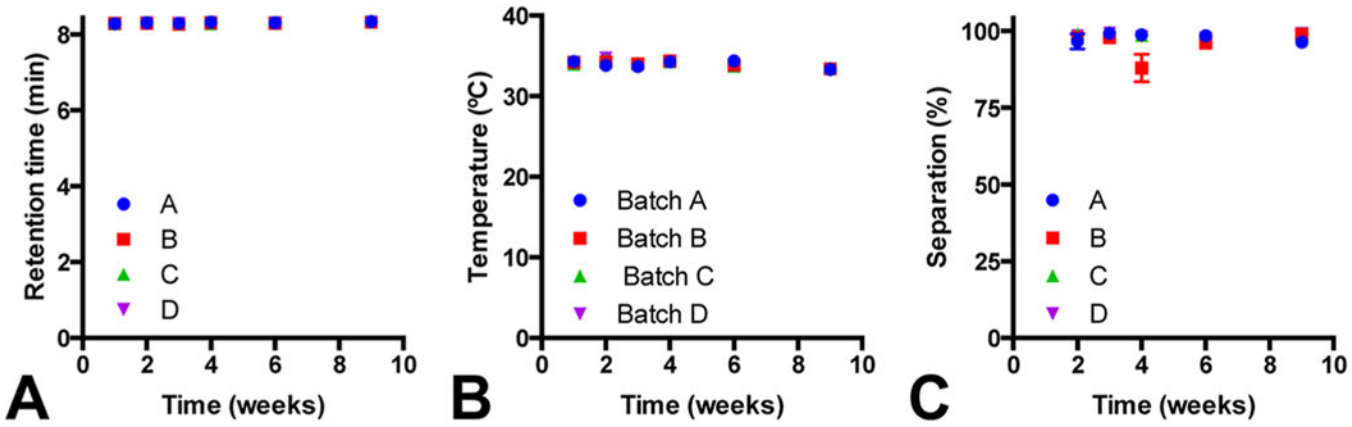

Figure 4.

Particle stability data for 2 month storage at room temperature. (A) SEC analysis shows the retention time for all particles remained constant around 8.3 min; (B) cloud point measurements shows the transition temperature for all particle remained constant around 34 °C; and (C) the magnetic separation efficiency for all particles at 40 °C was ≥95% (batch B week 4 was an outlier) over 2 month period.

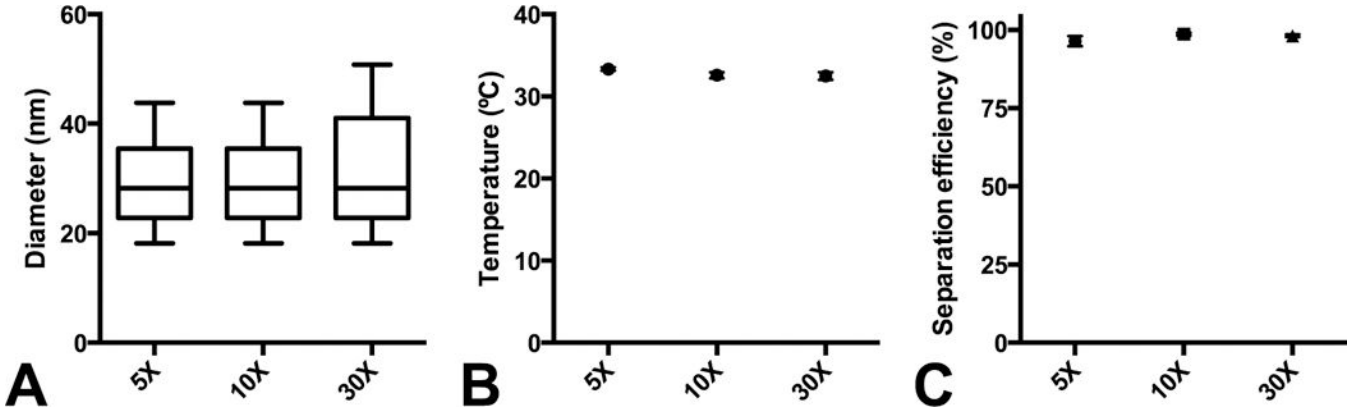

Figure 5.

Characterizations for scale-up particle synthesis. (A) Particle diameter distribution shows median diameter ~28 nm for all three syntheses. The 30× synthesis exhibits slighter wider diameter distribution, 18–50 nm. (B) Cloud point measurements show that the transition temperatures for all mNPs were ~34 °C. (C) All mNPs exhibit ≥95% magnetic separation efficiencies at 40 °C.

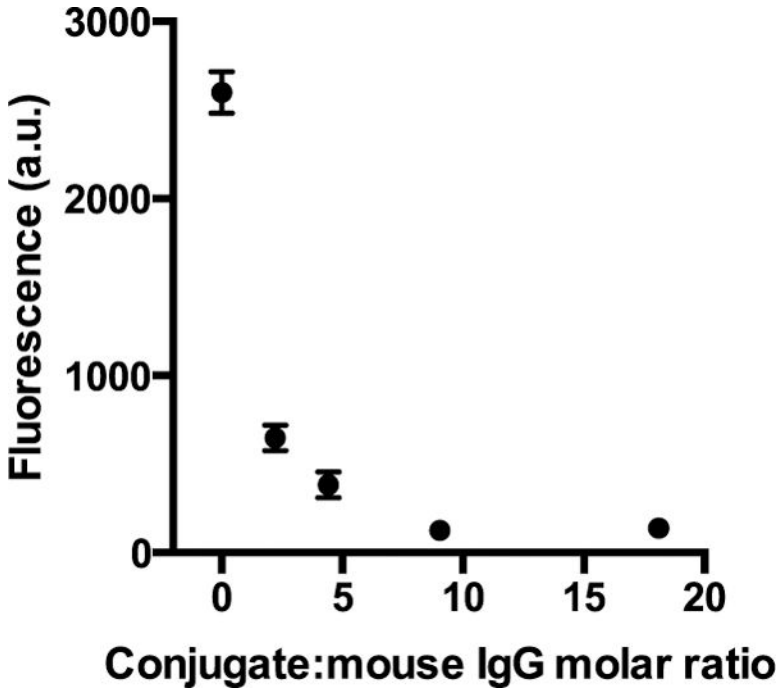

Figure 6.

Mouse IgG separation via the binary reagent system. Before the separation, the fluorescent intensity for the solution with 12.3 μg/ mL of mouse IgG was ~2600. After the magnetic separation, the solution fluorescent intensity reduced to ~650 when the conjugate/ mouse IgG ratio was 2.2:1. The signal reduced further when the conjugate/mouse IgG ratio was higher. The signal reached bottom when the conjugate/mouse IgG ratio was ≥9:1, which suggests that the separation was maximum.

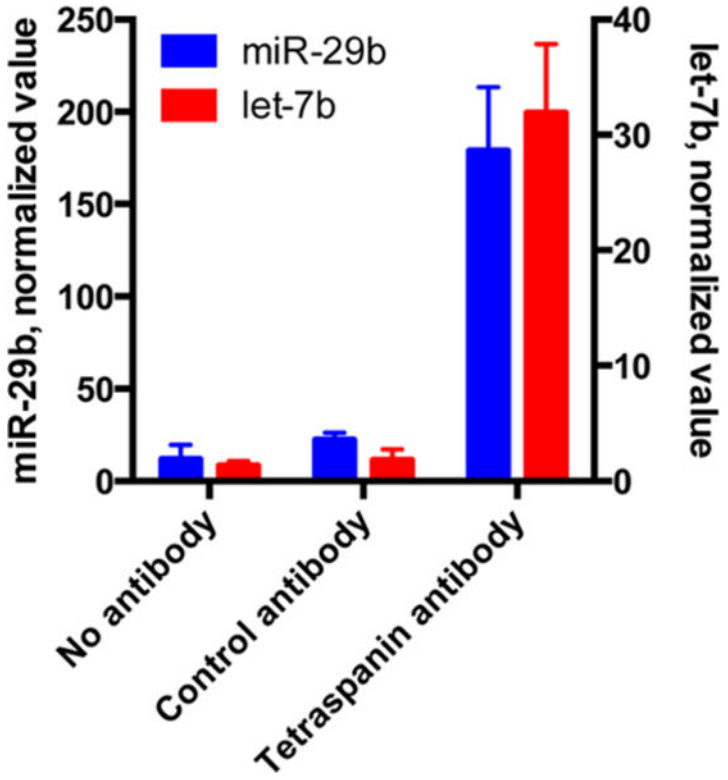

Figure 7.

EV-associated microRNAs are enhanced in samples selected using anti-tetraspanin antibodies in the binary reagent system. Total RNA was isolated from semen EV diluted to the same final volume as experimental samples, and samples purified in the binary reagent system using the specific control or exosome-specific anti-tetraspanin antibodies. Equal volumes of resulting RNA were subjected to reverse transcription and microRNA analysis using quantitative PCR. Results are normalized to a spike-in synthetic microRNA to normalize for differences in RNA extraction or reverse transcription efficiency. Normalized Ct values are compared to the mean result for diluted semen EV alone which is defined as 1. Results from three replicate experiments are plotted.

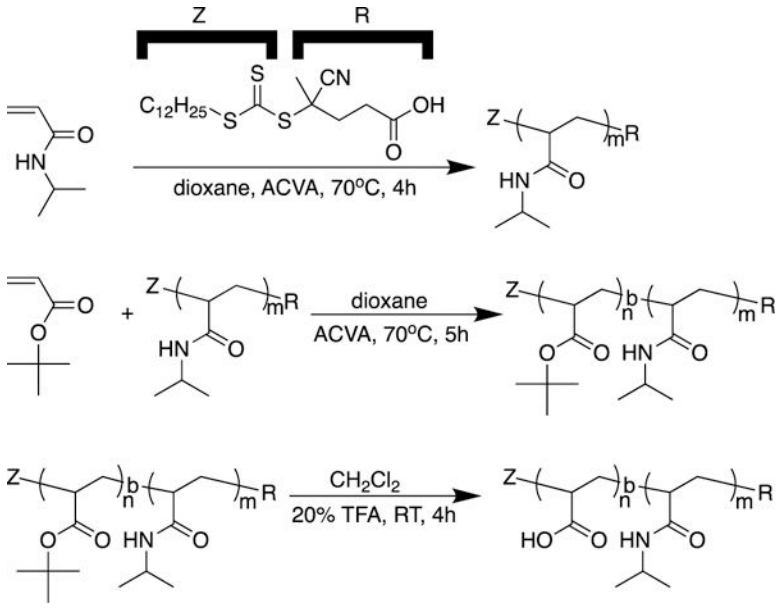

Scheme 1. RAFT-Mediated Synthesis of Diblock Copolymers Consisting of a Poly(N-isopropylacrylamide) (pNIPAAm, m = 163) Block and a Block Incorporating tert- Butyl Acrylate (t-BuA, n = 10)[a]

[a]The *tert*-butyl groups were cleaved by TFA treatment, which resulted in poly(acrylic acid)-*block*-poly(*N*-isopropylacrylamide).

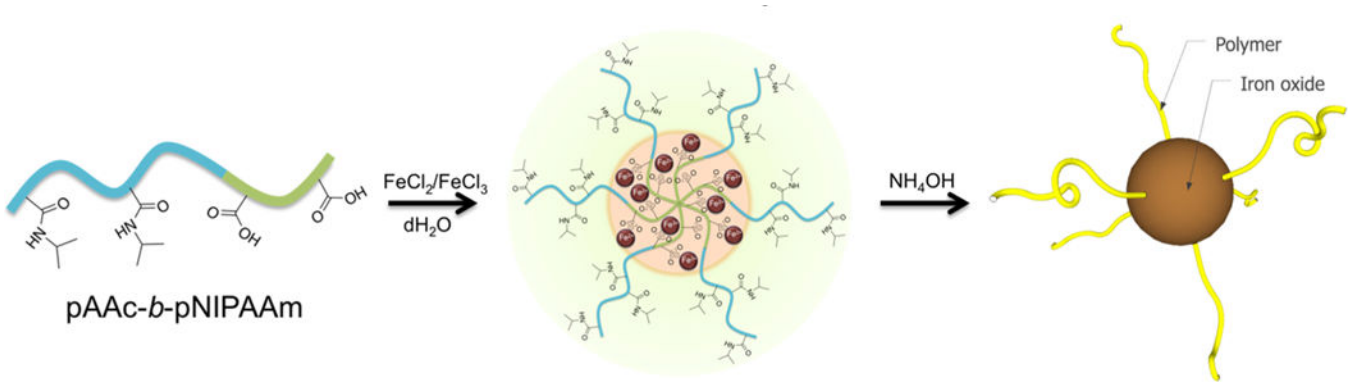

Scheme 2. Co-precipitation Synthesis of Temperature-Responsive Magnetic Nanoparticles[a]

[a]The RAFT-synthesized diblock co-polymer of pAAc-*b*-pNIPAAm complexes with iron cations (Fe^{2+}/Fe^{3+}) in water. Then, the addition of NH_4OH induced the iron oxide particle formation